Oxygen Reduction Reaction Catalyzed by Self-Assembled Monolayers of Copper-Based Electrocatalysts on a Polycrystalline Gold Surface

Masaru Kato,[†,‡] Nobuhisa Oyaizu,[‡] Katsuaki Shimazu,[†,‡] Ichizo Yagi[†,‡]*

[†]Faculty of Environmental Earth Science and [‡]Graduate School of Environmental Science, Hokkaido University, N10W5, Kita-ku, Sapporo 060-0810 Japan

Oxygen reduction reaction, copper complex, polymer electrolyte fuel cells, proton exchange membrane fuel cells, self-assembled monolayers, sum frequency generation spectroscopy

ABSTRACT (100-150 words)

We report two-dimensional model systems to study electrocatalytic activities of dinuclear copper complexes for various electrocatalytic reactions including the oxygen reduction reaction (ORR), where we can use electrochemical techniques as well as surface-sensitive techniques such as X-ray photoelectron spectroscopy and vibrational sum frequency generation spectroscopy. Heteroaromatic thiols including four triazoles and a thiadiazole are used as metal ligands as well as anchors to a polycrystalline gold electrode. The thiols are self-assembled on the polycrystalline gold elecctrode and then react with copper(II) ions to give monolayers of copper-based ORR catalysts on the surface. The dinuclear copper complexes of 1,2,4-triazole-3-thiol and 3-amino-1,2,4-triazole-5-thiol show ORR activity and similar pH-dependent catalytic behavior to that of counterparts supported on carbon black, suggesting that our two-dimensional systems can serve as model catalysts for carbon-supported molecular catalysts. We have also self-assembled dinuclear copper complexes with long alkyl or perfluoroalkyl chains on the surface and studied their orientation on the surface and oxygen transport.

INTRODUCTION

Polymer electrolyte fuel cells (PEFCs), also called polymer electrolyte membrane (PEM) fuel cells, efficiently convert hydrogen as a fuel into electricity through a chemical reaction with oxygen in the air. PEFCs are used for vehicles or home-use electricity generators. In the PEFCs, the oxygen reduction reaction (ORR) from dioxygen to water occurs at the cathode whereas hydrogen oxidation occurs at the anode. The ORR is a sluggish reaction and requires large overpotentials. For example, platinum group metal (PGM) catalysts have been used as ORR electrocatalysts in the state-of-the-art PEFCs. Although extensive efforts have been paid to develop PGM-based electrocatalysts,[1-10] these catalysts still require an overpotential of >0.2 V. Ideally we should develop ORR electrocatalysts with almost no overpotential to minimize the energy loss at the cathode. Furthermore, since PGMs are scarce and expensive, PGM catalysts should be replaced with earth-abundant catalysts for wide spread applications of PEFCs.

Although PGM catalysts drive the ORR in PEFCs, in nature metalloenzyes such as multi-copper oxidases (MCOs) efficiently catalyze the ORR with almost no overpotential.[11-14] MCOs have a multi-nuclear copper complex at the reaction center and this core structure inspires us to synthesize copper-based ORR catalysts.[15-24] An intriguing example of copper-based ORR catalysts is a dinuclear copper(II) complex of 3,5-diamino-1,2,4-triazole (Cu-Hdatrz).[20,25] Cu-Hdatrz supported on carbon black shows high ORR activity in the copper-based electrocatalysts (E_{onset} for ORR = 0.73 V vs pH 7)[20] and its ORR activity increases with increasing pH because of the faster ORR kinetics in basic solutions revealed by *in situ* X-ray absorption fine structure (XAFS) spectroscopy.[26] This ORR activity is far low, compared with that of PGM-based catalysts. Further improvement of the catalytic activity of copper-based catalysts is necessary for use in practical PEFCs.

To develop highly efficient ORR electrocatalysts, screening or mechanistic studies of the catalysts are required. However, these studies are not easy: we need multi-step preparation procedures for electrochemical measurements or observation of the ORR occurring at a three-phase interface. To study electrochemical ORR activity of molecular-based catalysts, the catalysts are generally immobilized on a carbon support with an ionomer: The conductive carbon support contacts with the catalyst and mediates electron transfer from the catalyst to the electrode surface. An ionomer plays important roles in binding carbon-support particles together and in proton or gas transport. In typical electrochemical experiments of ORR catalysts, many steps are required: synthesis of a catalyst, immobilization of the catalyst on a carbon support, drop-casting of the mixture of the catalyst and an ionomer on a glassy carbon disc electrode, and then electrochemical measurements of the electrode under oxygen. We need experienced preparation skills at each step to obtain reliable and reproducible electrochemical data. Such technical and time-intensive multi-steps are unsuitable for quick screenings of newly prepared electrocatalysts. Furthermore, the ORR catalyzed by the carbon-supported electrocatalyst occurs at the three-phase interface of the catalyst, the carbon support and the ionomer, making the mechanistic studies difficult. Thus, simple model systems, for example, two-dimensional systems, will allow us to simplify the electrode preparation process or to obtain mechanistic insights into the reaction mechanism or mass transport of oxygen or proton.[23,27-29]

Herein we report two-dimensional model systems to easily study the catalytic activity or oxygen transport of dinuclear copper-based ORR catalysts, which are based on Cu-Hdatrz. We have self-assembled heteroaromatic thiols (Chart 1) and then formed the copper-based ORR catalysts onto a polycrystalline gold surface. To characterize the self-assembled monolayers (SAMs) of the copper complexes, physical techniques are used including linear sweep

voltammetry, X-ray photoelectron spectroscopy (XPS) and vibrational sum frequency generation (VSFG) spectroscopy.

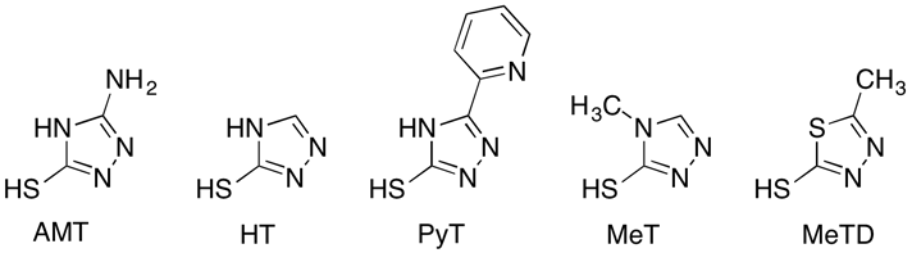

Chart 1. Chemical structures of the five-membered heteroaromatic thiols used in this work

EXPERIMENTAL METHODS

Materials. Perfluorotridecanoic acid 1*H*-1,2,4-triazole-3-thiol (HT), 5-(2-pyridyl)-4H-1,2,4-triazole-3-thiol (PyT), 4-methyl-4*H*-1,2,4-triazole-3-thiol (MeT) and *N*-hydroxysuccinimide (NHS) were purchased from Aldrich. Tridecanoic acid and 1-(3-dimethylaminopropyl)-3-ethylcarbodiimide hydrochloride (EDC·HCl) were commercially available from Tokyo Chemical Industry Co., Ltd. (TCI). The other chemicals including 3-amino-1,2,4-triazole-5-thiol (AMT), copper(II) sulfate pentahydrate ($CuSO_4 \cdot 5H_2O$) and 5-methyl-1,3,4-thiadiazole-2-thiol (MeTD) were purchased from Wako Pure Chemical Industries, Ltd. All chemicals were used without further purification.

Preparation of polycrystalline gold electrode substrates. A glass slide with a size of 1×2.6 cm was used as a substrate. The glass slide was heated at 210 °C, and then titanium was evaporated and deposited onto the glass slide at 0.1 nm s^{-1} under vacuum to obtain a titanium film with a thickness of >10 nm. The titanium film serves as an adhesion layer between gold and glass. A gold thin film with a thickness of ~150 nm was deposited onto the Ti-coated glass slides at 0.1 nm s^{-1} at room temperature under vacuum. Roughness factors of gold substrates were

determined from the charge required for the electrochemical reduction of the surface oxide in 0.1 M H_2SO_4. The roughness factors ranged from 1.1 to 1.6 depending on preparation lots. All surface or current densities were corrected based on the surface area considering the determined roughness factor. The corrected surface or current densities are shown in the main text.

Self-assembly of heteroaromatic thiols on the gold electrodes. We chose five heteroaromatic thiol compounds, AMT, HT, PyT, MeT and MeTD (Chart 1). Before the formation of these SAMs, gold electrode substrates were annealed over propane-oxygen flame and cooled in a nitrogen stream. The gold substrates were immersed in 3 mL of ethanol solution containing one of the thiol ligands (10 μM) and kept at 298 K under Ar for 0.5 h, 1 h, 5 h, 12 h or 24 h. The gold electrodes functionalized with the SAM were rinsed with ethanol and dried in a nitrogen stream. The prepared electrodes were immediately used for electrochemical measurements, functionalization with carboxylic acids, or complexation with Cu^{II} ions.

Complexation of copper(II) with the thiol SAMs on the gold electrodes. The thiol-functionalized gold electrodes were rinsed with Mili-Q water and dried in a nitrogen stream before complex formation with Cu^{II} ions. One of the thiol-gold electrodes was immersed in a 1 mM aqueous $CuSO_4$ solution (3 mL) and kept at 298 K under Ar for 24 h. The electrode was rinsed with Mili-Q, dried in a nitrogen stream and then used for further experiments.

Covalent bonding formation of perfluorotridecanoic acid or tridecanoic acid with the SAM of AMT on the gold substrate. Perfluorotridecanoic acid (0.0027 g, 0.0041 mmol), EDC·HCl (0.038 g, 0.20 mmol) and NHS (0.010 g, 0.087 mmol) were dissolved in 2 mL of an acetate buffered solution (pH 5.5) and the solution was sonicated for 1 h. In the case of tridecanoic acid, 2 mL of an acetate buffered solution (pH 5.5) containing 3wt% ethanol was

used. The solution was drop-cast onto the AMT-self-assembled gold substrate and kept at room temperature for 1 h. The substrate was rinsed with water, and dried in a nitrogen stream.

Electrochemistry. A typical three-electrode electrochemical system and a HZ-5000 Potentiostat (Hokuto Denko) were used for all electrochemical measurements. An Ag|AgCl reference electrode (saturated KCl) was used as a reference electrode. All potentials shown in this paper are converted to the reversible hydrogen electrode (RHE) using the following equation, $E_{RHE} = E_{Ag|AgCl} + 0.199 + pH \times 0.059$. A platinum plate covered with a platinum black film was used as a counter electrode. Britton-Robinson buffered electrolyte solutions at pH 4, 7 and 10 were purged with oxygen (purity, >99.5%) for >30 min before ORR measurements or purged with Ar (purity, >99.9995%) for >30 min before the other electrochemical measurements. In a 0.5 M KOH aqueous solution, the thiol SAMs were reductively desorbed from the gold electrode electrodes and the charges required for the reductive desorption allowed us to determine the amount of the thiol on the gold.

X-ray photoelectron spectroscopy (XPS). X-ray photoelectron spectra of the Cu-SAM electrodes were recorded on a JEOL JPS-9200 photoelectron spectrometer, where the take-off angle was set to 90°. The peak of Au $4f_{7/2}$ was used as the internal reference to calibrate the binding energies of the elements.

Contact angle measurements. The $\theta/2$ method was used to measure water contact angles. Milli-Q water (50 μL) was drop-cast on a substrate. Photographs of the side at the interface between the droplet and the substrate surface were taken by using a Nikon Digital Camera D3100. A water contact angle θ is determined from the apex of the water droplet and the contact point at the edge of the water droplet and the substrate (Figure S1).

Vibrational sum frequency generation (VSFG) spectroscopy. The VSFG spectra were recorded in the C−F stretching region (1250−1410 cm^{-1}) by a broadband femtosecond VSFG spectrometer consisting of a femtosecond Ti:sapphire oscillator/regenerative amplifier laser system (Integra-c, Quantronix), 100 fs, 2.35 mJ, 804 nm, 1 kHz. About 60% of the laser output was used to pump an optical parametric amplifier (OPA/OPG) system (TOPAS-c, Light Conversion, Inc.) to generate a broadband tunable IR beam with a bandwidth of ca. 200 cm^{-1} through an $AgGaS_2$ crystal for differential frequency generation (DFG). The remaining 40% of the broadband visible output at 804 nm was converted to a picosecond pulse tunable from the UV to near-IR region (220–1000 nm) by another OPA/OPG system (TOPAS-white-NB, Light Conversion, Inc.). Typically, visible wavelength of 600 nm was selected for narrow-band visible beam in the present study. The visible and infrared beams overlapped in a copropagating geometry on the substrate with incident angles of 65° and 50°, respectively. The SFG signal was dispersed through a monochromator (MS3501i, Solar-TII) and collected by a charge-coupled device (CCD) camera (DU420A-BU2, Andor Technology) equipped with a Peltier cooler. The VSFG spectra were recorded in ppp (in the order of SFG, Vis, IR) polarization combination and were accumulated for 3 min. The intensities of the SFG spectra were normalized by VSFG spectra obtained at a clean gold substrate with an acquisition time of 1 min. To cover the frequency region mentioned above, broadband VSFG spectra collected at the 4 or 5 different center wavelengths of IR were required and the properly normalized spectra can be connected without any further corrections.

RESULTS AND DISCUSSION

We have prepared SAMs of the heteroaromatic thiols, AMT, HT, PyT, MeT and MeTD (**Chart 1**) and coordinated copper(II) ions to them on the polycrystalline gold substrates to

obtain two-dimensional ORR model systems. We chose these five heteroaromatic ligands considering Hdatrz, which is used as a ligand in the Cu-Hdatrz catalyst.[20] Hdatrz has a 1,2,4-triazole ring and two amino groups at the 3- and 5-positions. AMT has a similar structure to Hdatrz but the thiol group, which is required to form a SAM of AMT on Au. HT, PyT and MeT have also one 1,2,4-triazole ring and one thiol group but with a different functional group: –H for HT, –2-pyridyl for PyT and –Me for MeT. MeTD has one 1,3,4-thiadiazole ring, not a triazole ring.

The SAMs of the hteteroaromatic thiols were easily obtained on the polycrystalline gold substrate: the polycrystalline gold substrate was immersed in an ethanol solution containing each ligand (10 μM) and kept at 298 K under Ar for 24 h. XPS spectra of the thiol-functionalized substrates showed peaks in the N1s and S1s region, indicating the formation of the thiol SAMs on Au, whereas no peak was observed for the bare Au substrate (**Figure S2**). Electrochemical measurements on the reductive desorption of the thiol SAMs from Au revealed that an immersion time of at least 24 h was required to obtain the stabilized SAMs (**Figure S3**). **Figure 1** shows linear-sweep voltammograms on the reductive desorption of the monolayers formed after 24 h of immersion. Each voltammogram has at least two reduction peaks. Similar linear-sweep voltammograms were reported on reductive desorption of heteroaromatic thiols such as 5-amino-1,3,4-thiadiazole-2-thiol.[30]

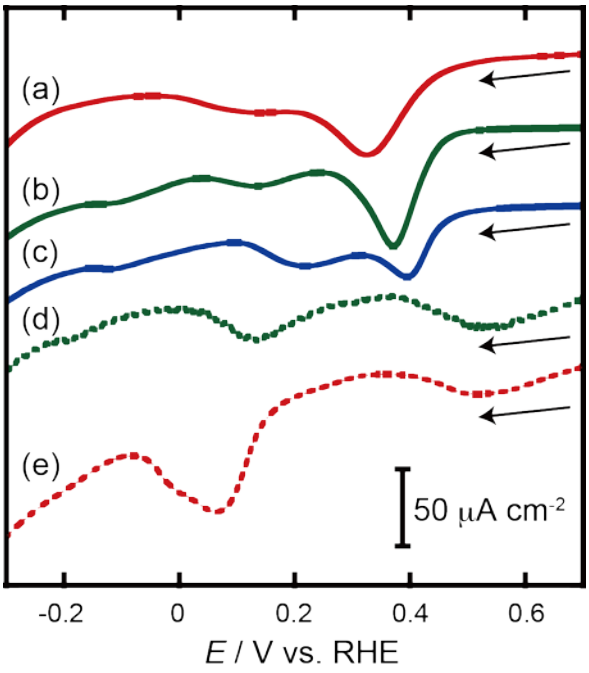

Figure 1. Reductive desorption voltammograms of (a) AMT, (b) HT, (c) PyT, (d) MeT and (e) MeTD from Au, recorded at a sweep rate of 0.1 V s^{-1} in 0.5 M KOH aqueous solution. The electrodes were immersed and kept in the ethanol solution containing each thiol ligand for 24 h. The arrows indicate the scanning direction.

The integration of the reduction waves in **Figure 1** gave surface coverage of the thiols: $(6.3\pm0.1)\times10^{-10}$ mol cm^{-2} for AMT; $(6.2\pm0.1)\times10^{-10}$ mol cm^{-2} for HT; $(5.4\pm0.1)\times10^{-10}$ mol cm^{-2} for PyT; $(5.8\pm0.1)\times10^{-10}$ mol cm^{-2} for MeT and $(6.3\pm0.1)\times10^{-10}$ mol cm^{-2} for MeTD. These surface coverages are slightly lower than those of the reported monolayers of MeT (7.5×10^{-10} mol cm^{-2}),[30] indicating that the heteroaromatic thiols formed submonolayers on the polycrystalline gold substrate, where the heteroaromatic thiol may interact with the gold surface not only thorough the sulfur atom but also through nitrogen atoms of the five-membered ring.

The gold substrates modified with the heteroaromatic thiols were immersed in aqueous solution containing $CuSO_4$ (1 mM) and kept at room temperature for 24 hours under Ar to obtain copper(II) complexes of the heteroaromatic thiols on the gold surface. Cyclic voltammograms of

the resulting electrodes allowed us to confirm the formation of copper complexes for AMT, HT and PyT, but not for MeT and MeTD. **Figure 2** shows representative cyclic voltammograms of Cu-AMT, Cu-HT and Cu-PyT recorded in a degassed Britton-Robinson buffered solution at pH 7. The voltammograms showed an oxidation peak at ca. +0.85 V vs RHE and a reduction peak at ca. +0.75 V vs RHE, assigned to $Cu^{II/I}$ redox couples, whereas such redox couples were not observed in the case of MeT or MeTD (**Figure S4**). Cu-AMT showed an oxidative current at higher potentials (> +1 V vs RHE) as well, which is due to polymerization of AMT on the electrode.[31] Plots of current density at the reduction peak against sweep rate gave linear relationships for Cu-AMT, Cu-HT and Cu-PyT (**Figure 2**, inset), suggesting that these copper complexes were immobilized on the gold surface. We also recorded reduction desorption voltammograms of Cu-AMT, Cu-HT and Cu-PyT and observed negative shifts of the reduction peaks attributed to reductive desorption, indicating copper complex formation (**Figure S5**).

Interestingly, MeT or MeTD showed no complexation with copper(II) ions on the surface. It seems that the nitrogen at the 4-position plays an important role in the complexation on the surface. AMT, HT or PyT has the 1,2,4-triazole ring with the unfunctionalized nitrogen at the 4-position, whereas the 4-position nitrogen of MeT is functionalized with the methyl group and MeTD has no triazone ring. Such structural difference might cause changes in the surface orientation for MeT and MeTD, resulting in no complexation with copper(II) ions.

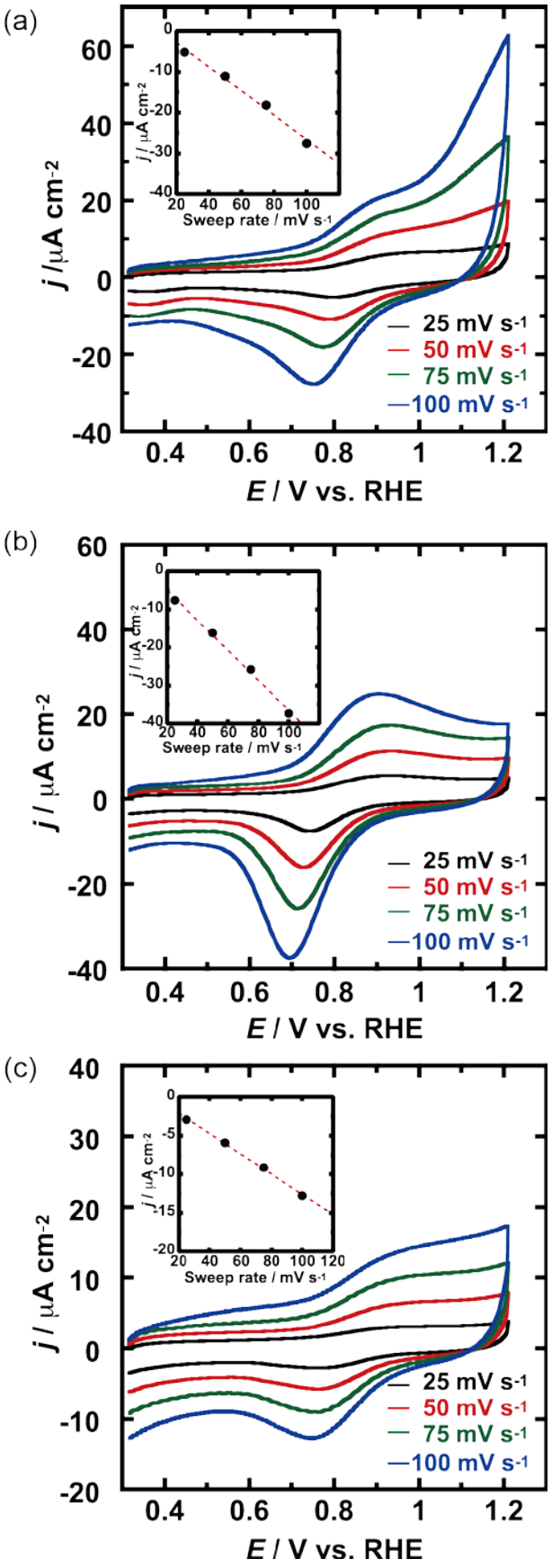
(a)
j /μA cm-2
E / V vs. RHE
25 mV s-1
50 mV s-1
75 mV s-1
100 mV s-1
j / μA cm-2
Sweep rate / mV s-1
(b)
j / μA cm-2
E / V vs. RHE
25 mV s-1
50 mV s-1
75 mV s-1
100 mV s-1
j / μA cm-2
Sweep rate / mV s-1
(c)
j / μA cm-2
E / V vs. RHE
25 mV s-1
50 mV s-1
75 mV s-1
100 mV s-1
j / μA cm-2
Sweep rate / mV s-1

Figure 2. Sweep-rate-dependent cyclic voltammograms of the gold electrodes functionalized with the SAMs of (a) Cu-AMT, (b) Cu-HT and (c) Cu-PyT. The cyclic voltammograms were recorded in a Britton-Robinson buffered solution at pH 7 under Ar. The insets show plots of current density against sweeping rate.

The surface coverages of copper complexes were determined from the charges passed upon the redox of the complexes (**Figure 2**) to be 3.1×10^{-10} mol cm^{-2} for Cu-AMT, 3.5×10^{-10} mol cm^{-2} for Cu-HT and 1.2×10^{-10} mol cm^{-2} for Cu-PyT. Considering the surface coverages of the submonolayers of the heteroaromatic thiols on Au electrodes (see above), we determined copper-to-ligand ratios to be approximately 1:2 for Cu-AMT and Cu-HT but to be 1:5 for Cu-PyT. The surface density of copper ions for Cu-PyT is much less than those for Cu-AMT and Cu-HT. The additional nitrogen-donating atom and/or the steric hindrance of the 2-pyridyl group might prevent PyT from the copper complex formation on the gold surface.

XPS analysis in the Cu $2p_{3/2}$ region also supports the formation of copper complexes of AMT, HT and PyT on Au. The XPS spectra of the Cu complexes of AMT, HT and PyT on the gold surface were deconvoluted into two peaks: 932.78 eV and 935.46 eV for Cu-AMT; 932.84 and 935.42 eV for Cu-HT; 932.78 eV and 935.46 eV for Cu-PyT (**Figure 3**). In contrast, one peak was observed at 932.77 eV for Cu-MeT or at 932.78 eV for Cu-MeTD (**Figure S6**). For a control experiment, a bare gold substrate was immerse into the aqueous solution containing copper(II) ion, rinsed with Milli-Q water, dried in a N_2 stream , followed by XPS measurements. This gold substrate also exhibited a peak at 932.84 eV in the Cu $2p_{3/2}$ XPS spectrum. Thus, the peaks observed around 932.8 eV might be attributed to cuprous oxide (Cu_2O) or metal copper.[32-34]

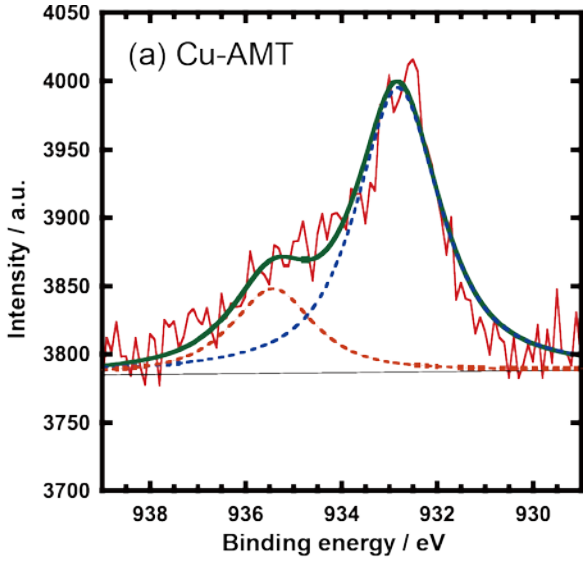
(a) Cu-AMT
Intensity / a.u.
4050
4000
3950
3900
3850
3800
3750
3700
938
936
934
932
930
Binding energy / eV

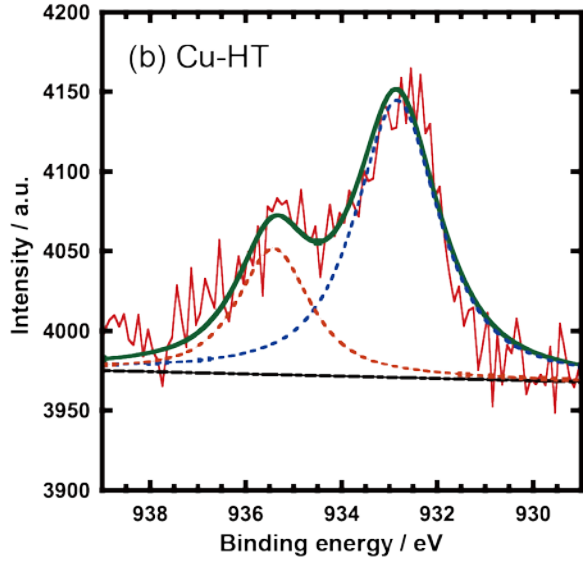
(b) Cu-HT
Intensity / a.u.
4200
4150
4100
4050
4000
3950
3900
938
936
934
932
930
Binding energy / eV

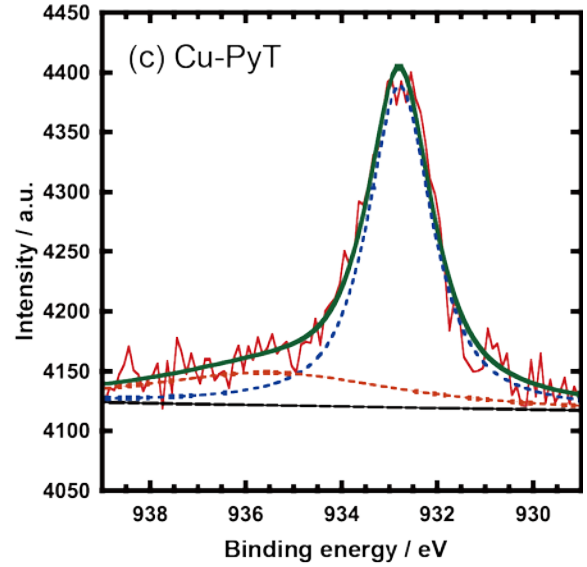
(c) Cu-PyT
Intensity / a.u.
4450
4400
4350
4300
4250
4200
4150
4100
4050
938
936
934
932
930
Binding energy / eV

Figure 3. XPS spectra of the Cu $2p_{3/2}$ region of (a) Cu-AMT, (b) Cu-HT and (c) Cu-PyT on gold.

The ORR activity of the copper complexes on Au electrodes was investigated at pH 7 under oxygen. Linear-sweep voltammograms show that Cu-AMT and Cu-HT have similar onset potentials for the ORR, +0.74 V vs RHE for Cu-AMT and +0.72 V vs RHE for Cu-HT (**Figure 4**), indicating that Cu-AMT and CuHT have similar ORR activity. Cu-PyT shows a lower onset potential of +0.65 V vs RHE, compared with Cu-AMT and Cu-HT. Thus, the difference in the functional group of $–NH_2$ in AMT and –H in HT is not sensitive to the ORR activity, but the 2-pyridyl group suppresses the ORR activity. Note that similar effects of functional groups on onset potentials were previously reported: +0.73 V vs. RHE for the carbon-supported Cu-Hdatrz, which is the counterpart of Cu-AMT/Au, and +0.70 V vs. RHE for a carbon-supported Cu-Htrz (Htrz = 1,2,4-triazole), which is the counterpart of Cu-HT/Au.[15] These results imply that our two-dimensional systems work as model systems of the copper-based ORR catalysts supported on carbon black.

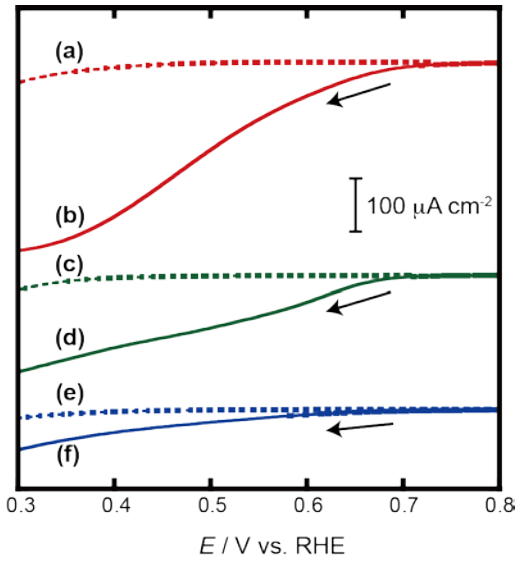

Figure 4. LSVs of (a) AMT/Au (the dotted line in red), (b) Cu-AMT/Au (the solid line in red), (c) HT/Au (the dotted line in green), (d) Cu-HT/Au (the solid line in green), (e) PyT/Au (the

dotted line in blue) and (f) Cu-PyT/Au (the solid line in blue). All LSVs were recorded in a 40 mM Britton-Robbinson buffered aqueous solution containing 0.1 M $NaClO_4$ (pH 7) at a scanning rate of 20 mV s^{-1} under oxygen. The arrows indicate the scanning direction.

Interestingly, the observed onset potentials of Cu-AMT/Au and Cu-HT/Au seem slightly greater than their corresponding carbon supported catalysts of Cu-Hdatrz and Cu-Htrz. In our two-dimensional model system, the triazole ring possesses a thiol group that is directly connected to the triazole ring, and the redox center of the copper complex may be placed close to the electrode surface. Such a zero-chain thiol may facilitate the interfacial electron transfer from the electrode surface to the redox center and eliminate the interfacial electron transfer as the rate-limiting step for ORR.[27,35]

We recorded linear sweep voltammograms of Cu-AMT and Cu-HT in the pH range from pH 4 to pH 13 under oxygen (**Figure 5**). Onset potentials for the ORR increased with increasing pH with slopes of (+0.036 V vs RHE)/pH for Cu-AMT and (+0.035 V vs RHE)/pH for Cu-HT, which are equivalent to (-0.024 V vs Ag|AgCl)/pH for Cu-AMT and (-0.025 V vs Ag|AgCl)/pH for Cu-HT. These values are approximately half the value of -0.059 V/pH predicted by the Nernst equation for a reaction involving the transfer of one proton and two electrons, implying that the rate-determining step involves the transfer of one proton and two electrons. Similar pH-dependence was reported on the carbon-supported Cu-Hdatrz,[20,26] suggesting that the rete-determining step of the carbon-supported Cu-Hdatrz is the same as those of Cu-AMT/Au and Cu-HT/Au. Thus, it is most likely that Cu-AMT/Au and Cu-HT/Au have a dinuclear copper core similar to the core of Cu-Hdatrz.

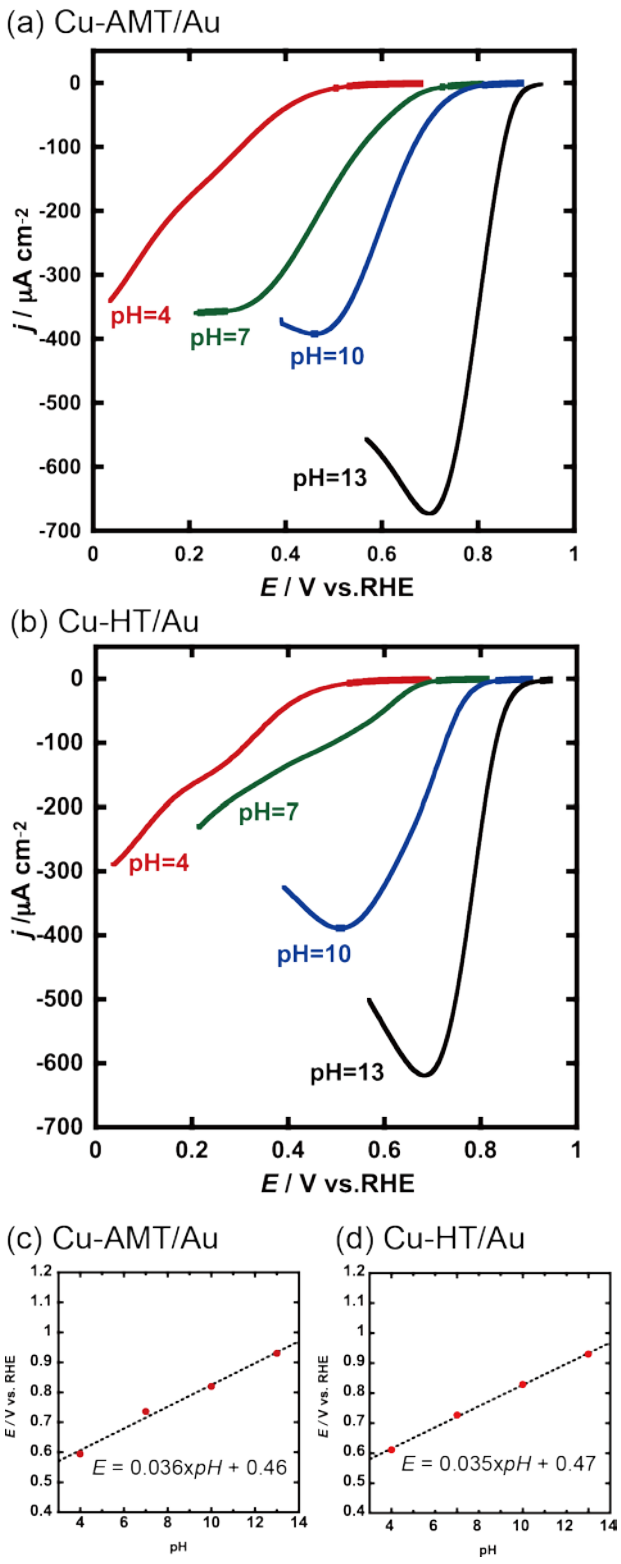

Figure 5. Linear-sweep voltammograms of (A) Cu-AMT/Au and (B) Cu-HT/Au in electrolytes of varying pH under oxygen. All linear-sweep voltammograms were negatively scanned at a

scanning rate of 20 mV s^{-1}. Plots of the onset potentials of ORR against pH (C) for Cu-AMT/Au and (D) Cu-HT/Au.

To gain insights into the orientation of the copper complexes on the surface, we have performed VSFG spectroscopy of AMT/Au and Cu-AMT/Au. VSFG spectroscopy is a powerful technique to understand orientations of molecules or polymers immobilized on surfaces.[36] We recorded VSFG spectra in the range from 1250 cm^{-1} to 1400 cm^{-1}, probably including C=C and N-C stretching bands in triazoles, and obtained only a broad peak at around 1300 cm^{-1} for AMT/Au or Cu-AMT/Au (**Figure 6a**), which can be assigned to the asymmetric N-C stretching band of triazole ring. Some peaks on the triazole ring should be observed when the triazole ring is oriented vertically to the surface. Thus, the core structure consisting of two copper(II) ions and two triazoles as bridging ligands should be immobilized out of the vertical to the surface. Similar results were reported on SAMs of AMT on Ag or Au.[37] Further VSFG measurements in the lower frequency region including N-N stretching band are required to confirm the orientation of the 1,2,4-triazole ring.

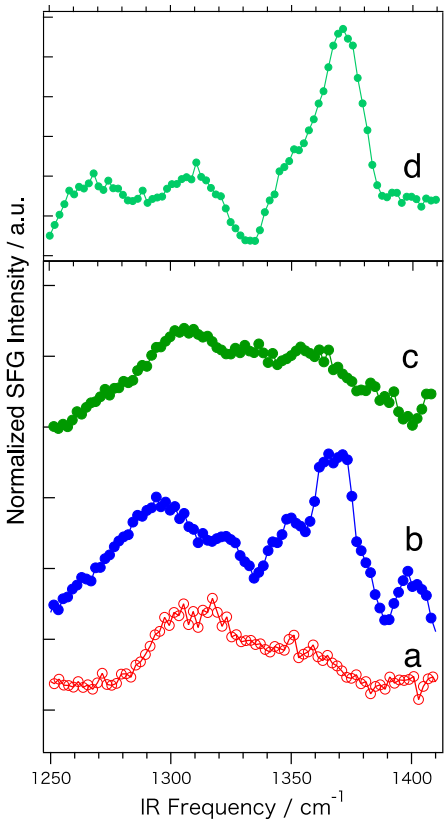

Figure 6. VSFG spectra of (a) AMT/Au, (b) CFAMT/Au, (c) Cu-CFAMT/Au and (d) 1*H*, 1*H*, 2*H*, 2*H*-Perfluorodecanethiol/Au.

Analysis on the surface coverage, pH-dependence of ORR and VSFG spectra allows us to confirm the formation of the Cu-AMT and Cu-HT sub-monolayers on the gold surface (**Scheme 1**). These copper complexes have a dinuclear copper core linked with two triazoles working as bridging ligands, where the copper-to-ligand-ratio is 1:1. As mentioned above, the copper-to-ligand ratio determined from the surface coverage is 1:2. Therefore, ca. 50% of the triazole molecules immobilized on the surface are used for the complexation with copper(II) ions.

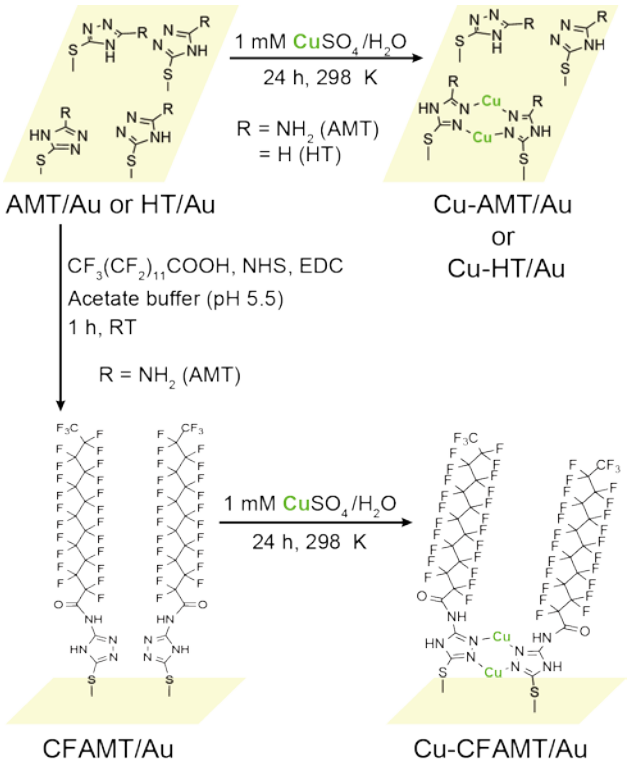

Scheme 1. Schematic representation of self-assembly of copper-based ORR catalysts on the polycrystalline gold surfaces.

To understand environmental influences of Cu-AMT on the ORR activity, we covalently functionalize Cu-AMT/Au with long perfluoroalkyl or alkyl chains. In practical PEFCs, ionomers are used as proton/oxygen transporter from the bulk solution to the reaction center of the electrocatalyst for ORR. Nafion, which is an ionomer widely used, has a perfluoroalkyl main chain with side chains of perfluorosulfonic acid. The functionalization of Cu-AMT with a perfuluoroalkyl chain will allow us to unveil the role of Nafion on ORR catalytic activity through our two-dimensional model systems.

We have covalently grafted a perfluorotridecanyl chain at the amino group of AMT/Au to obtain a SAM of AMT-perfluorotridecanoamide on Au (CFAMT/Au) and then reacted the SAM with copper(II) ions, resulting in the formation of a copper complex of CFAMT on Au (Cu-

CFAMT/Au, **Scheme 1**). We have also prepared a copper complex of AMT-tridecanoamide on the gold substrate (Cu-CHAMT/Au) in the same synthetic procedure. The long-chain functionalized AMT and Cu-AMT SAMs were characterized using XPS, wettability and VSFG spectroscopy measurements.

XPS and wettability measurements revealed the formation of the CFAMT SAM on the gold substrate. A peak was observed in the F 1s region of XPS spectra for CFAMT/Au or Cu-CFAMT, whereas no peak was observed for a bare Au substrate or AMT/Au (**Figure S7**). The perfluorotridecanyl chain forms covalent bonding with AMT on the gold substrate. The wettability measurements enable us to determine a contact angle (θ) of 29±1° for CFAMT/Au and that of 8.3±0.7° for AMT/Au (**Figure S8**), indicating that the surface of CFAMT/Au is clearly hydrophobic, compared with the unfunctionalized AMT/Au. This result also supports the formation of CFAMT/Au.

VSFG spectroscopy of CFAMT/Au provided the evidence on the vertical orientation of CFAMT SAMs to the gold surface. A VSFG spectrum of CFAMT/Au shows peaks at 1350 cm^{-1} and 1370 cm^{-1}, which can be assigned to the symmetric C-F_3 stretching vibration of the terminal CF_3 group[38] (**Figure 6**). For comparison, a VSFG spectrum of a SAM of 1*H*,1*H*,2*H*,2*H*-perfluorodecanethiol on Au, which is known to form a densely packed SAM on Au,[39-40] was recorded and also showed peaks at the same positions (**Figure 6**), suggesting that CFAMT/Au is vertically oriented to the surface.

We also recorded a VSFG spectrum of Cu-CFAMT/Au. It is clear that the peak intensity of CFAMT/Au is greater than that of Cu-CFAMT/Au (**Figure 6**), indicating that the copper complex formation of CFAMT may cause conformational changes. The VSFG peak intensity correlates with the orientation of an immobilized compound on the surface. The VSFG peak

intensity of the terminal $-CF_3$ maximizes when the back-born of the SAM molecule has an angle of 90° with the surface; the CF_3 symmetric vibrational peak intensity decreases with decreasing the angle of the perfluoroalkyl chain with the surface. Thus, the copper complex formation decreases the angle of perfluoroalkyl chain of CFAMT/Au with the surface.

To investigate the influence of the perfluoro-group on the ORR activity, we recorded linear sweep voltammograms of Cu-CFAMT and Cu-CHAMT in the pH range between pH 4 and pH 13 (**Figure 7**). The pH dependence of Cu-CFAMT and Cu-CHAMT on ORR activity gave linear relationships (**Figures 7b** and **7c**), which are quite similar to those of Cu-AMT and Cu-HT (**Figure 5**). These results indicate that the reaction mechanism of the catalytic core of the copper site for ORR is the same for Cu-AMT/Au, Cu-CFAMT/Au and Cu-CHAMT/Au.

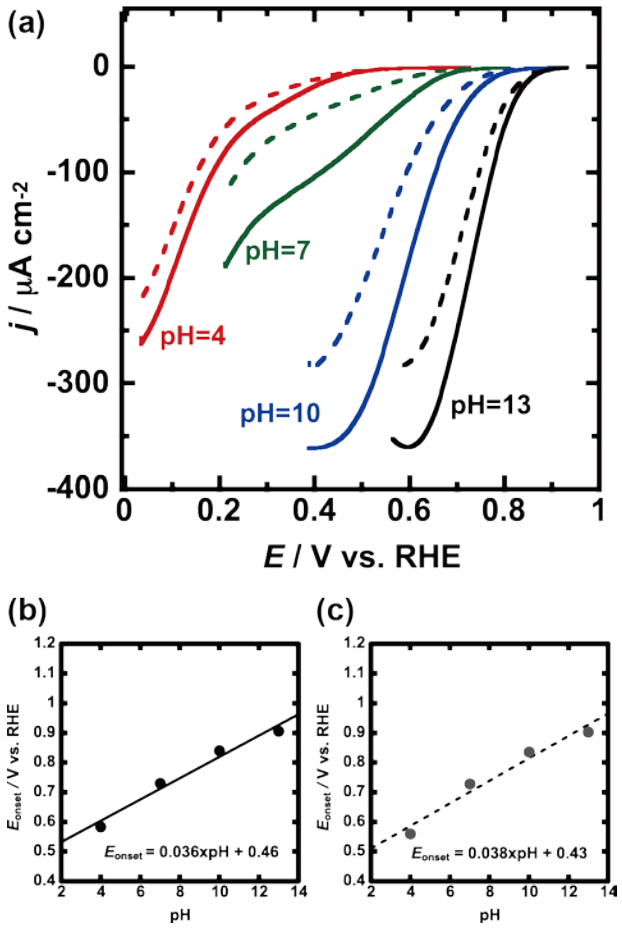

Figure 7. (a) Linear sweep voltammograms of Cu-CF-AMT/Au (solid traces) and Cu-CH-AMT/Au (dotted traces) and pH-dependence of onset potentials for ORR determined for (b) Cu-CF-AMT/Au and (c) Cu-CH-AMT/Au.

Interestingly, Cu-CFAMT shows higher current densities than Cu-CHAMT does. Cu-CFAMT might have higher oxygen mass-transfer (diffusion) property than Cu-CHAMT because oxygen permeability in fluorinated compounds is higher than that in alkyl compounds.[41] This result may imply that fluorocarbon environments around ORR catalytic cores can improve the oxygen transport. Such improvement on oxygen transport may be also observed in practical ORR systems containing perfluoroalkyl polymers such as Nafion.

CONCLUSIONS

We have developed the two-dimensional model systems to understand the electrocatalytic activity of the dinuclear copper ORR catalysts in detail. The heteroaromatic thiols used form the SAMs on Au, and the three thiols of them, AMT, HT and PyT, form copper complexes on the surface. The Cu-AMT/Au and Cu-HT/Au show greater ORR activity than the Cu-PyT/Au does in terms of the onset potential, suggesting that functional groups play key roles in the formation of the catalytically active dinuclear copper cores and modulation of the catalytic ORR activity. Furthermore, the pH-dependence on the ORR catalytic activity of Cu-AMT/Au and Cu-HT/Au is the same as that of carbon-supported counterparts. Thus, our two-dimensional systems can be used as model systems to carbon-supported dinuclear copper complexes for ORR.

One of the great advantages on our two-dimensional model systems is that electrochemical and surface-sensitive physical techniques can be applied to them. In practical ORR systems including carbon-supported ORR catalysts co-immobilized with an ionomer, it is difficult to understand, for example, the orientation of the catalysts on the carbon-support or mass transport systematically. We have compared the self-assembled Cu-AMT/Au, Cu-CFAMT/Au and Cu-CHAMT/Au from the viewpoints of catalytic activity, orientation on the surface and oxygen transport. Although these catalysts showed similar pH-dependent behavior on ORR, Cu-CFAMT/Au showed higher current densities than Cu-CHAMT/Au did, indicating that functional groups give no effect on the reaction mechanism as long as the dinuclear core structure is the same, but give some effects on oxygen transport.

Our findings in this work suggest that the functional groups of the 1,2,4-triazole ligands affect the dinuclear complex formation, the orientation of the catalysts and oxygen permeability, but give a marginal effect on the ORR catalytic activity. In other words, to drastically improve the catalytic activity of copper complexes of triazole ligands, new catalysts with a different catalytic core should be designed and synthesized, for example, trinuclear copper complexes, which are inspired by the catalytic reaction center of laccases, or multinuclear transition metal complexes such as iron and cobalt with triazoles.

In this work we have studied molecular-based electrocatalysts for ORR though our two-dimensional systems. In principle, our system can be applied to other electrocatalysts that drive other electrocatalytic reactions, for example, proton reduction. Further work is currently underway to find highly active electrocatalysts using our two-dimensional systems.

ACKNOWLEDGMENT

The authors would like to thank MEXT Program for Development of Environmental Technology using Nanotechnology from the Ministry of Education, Culture, Sports, Science and Technology, Japan for their financial supports.

Supporting Information. XPS, wettability, and LSVs at various SAMs are shown. This material is available free of charge via the Internet at http://pubs.acs.org.

AUTHOR INFORMATION

Corresponding Author

*E-mail: iyagi@ees.hokudai.ac.jp; Phone: +81-(0)11-706-4526

REFERENCES

(1) Huang, X. Q.; Zhao, Z. P.; Cao, L.; Chen, Y.; Zhu, E. B.; Lin, Z. Y.; Li, M. F.; Yan, A. M.; Zettl, A.; Wang, Y. M., *et al.* High-Performance Transition Metal-Doped Pt3ni Octahedra for Oxygen Reduction Reaction. *Science* **2015,** *348*, 1230-1234.
(2) Ma, L.; Wang, C. M.; Xia, B. Y.; Mao, K. K.; He, J. W.; Wu, X. J.; Xiong, Y. J.; Lou, X. W. Platinum Multicubes Prepared by Ni2+-Mediated Shape Evolution Exhibit High Electrocatalytic Activity for Oxygen Reduction. *Angew. Chem. Int. Ed.* **2015,** *54*, 5666-5671.
(3) Cui, C. H.; Gan, L.; Heggen, M.; Rudi, S.; Strasser, P. Compositional Segregation in Shaped Pt Alloy Nanoparticles and Their Structural Behaviour During Electrocatalysis. *Nat. Mater.* **2013,** *12*, 765-771.
(4) Chen, C.; Kang, Y. J.; Huo, Z. Y.; Zhu, Z. W.; Huang, W. Y.; Xin, H. L. L.; Snyder, J. D.; Li, D. G.; Herron, J. A.; Mavrikakis, M., *et al.* Highly Crystalline Multimetallic Nanoframes with Three-Dimensional Electrocatalytic Surfaces. *Science* **2014,** *343*, 1339-1343.
(5) Zhang, D. F.; Li, J.; Kang, J. X.; Chen, T. W.; Zhang, Y.; Wang, L. L.; Guo, L. From Pt-Rich Dendrites to Ni-Rich Cuboctahedrons: Structural Evolution and Electrocatalytic Property Studies. *CrystEngComm* **2014,** *16*, 5331-5337.
(6) Zhang, L.; Roling, L. T.; Wang, X.; Vara, M.; Chi, M. F.; Liu, J. Y.; Choi, S. I.; Park, J.; Herron, J. A.; Xie, Z. X., *et al.* Platinum-Based Nanocages with Subnanometer-Thick Walls and Well-Defined, Controllable Facets. *Science* **2015,** *349*, 412-416.
(7) Wang, D. L.; Xin, H. L. L.; Hovden, R.; Wang, H. S.; Yu, Y. C.; Muller, D. A.; DiSalvo, F. J.; Abruna, H. D. Structurally Ordered Intermetallic Platinum-Cobalt Core-Shell Nanoparticles with Enhanced Activity and Stability as Oxygen Reduction Electrocatalysts. *Nat. Mater.* **2013,** *12*, 81-87.
(8) Wu, Y. E.; Wang, D. S.; Zhou, G.; Yu, R.; Chen, C.; Li, Y. D. Sophisticated Construction of Au Islands on Pt-Ni: An Ideal Trimetallic Nanoframe Catalyst. *J. Am. Chem. Soc.* **2014,** *136*, 11594-11597.
(9) Nie, Y.; Li, L.; Wei, Z. D. Recent Advancements in Pt and Pt-Free Catalysts for Oxygen Reduction Reaction. *Chem. Soc. Rev.* **2015,** *44*, 2168-2201.
(10) Liu, H. L.; Nosheen, F.; Wang, X. Noble Metal Alloy Complex Nanostructures: Controllable Synthesis and Their Electrochemical Property. *Chem. Soc. Rev.* **2015,** *44*, 3056-3078.
(11) Mano, N.; Soukharev, V.; Heller, A. A Laccase-Wiring Redox Hydrogel for Efficient Catalysis of O_2 Electroreduction. *J. Phys. Chem. B* **2006,** *110*, 11180-11187.
(12) Kjaergaard, C. H.; Rossmeisl, J.; Norskov, J. K. Enzymatic Versus Inorganic Oxygen Reduction Catalysts: Comparison of the Energy Levels in a Free-Energy Scheme. *Inorg. Chem.* **2010,** *49*, 3567-3572.
(13) Thorum, M. S.; Anderson, C. A.; Hatch, J. J.; Campbell, A. S.; Marshall, N. M.; Zimmerman, S. C.; Lu, Y.; Gewirth, A. A. Direct, Electrocatalytic Oxygen Reduction by Laccase on Anthracene-2-Methanethiol-Modified Gold. *J. Phys. Chem. Lett.* **2010,** *1*, 2251-2254.
(14) Blanford, C. F.; Heath, R. S.; Armstrong, F. A. A Stable Electrode for High-Potential, Electrocatalytic O_2 Reduction Based on Rational Attachment of a Blue Copper Oxidase to a Graphite Surface. *Chem. Commun.* **2007**, 1710-1712.
(15) Thorseth, M. A.; Tornow, C. E.; Tse, E. C. M.; Gewirth, A. A. Cu Complexes That Catalyze the Oxygen Reduction Reaction. *Coord. Chem. Rev.* **2013,** *257*, 130-139.

(16) Xi, Y. T.; Wei, P. J.; Wang, R. C.; Liu, J. G. Bio-Inspired Multinuclear Copper Complexes Covalently Immobilized on Reduced Graphene Oxide as Efficient Electrocatalysts for the Oxygen Reduction Reaction. *Chem. Commun.* **2015,** *51*, 7455-7458.
(17) Tahsini, L.; Kotani, H.; Lee, Y. M.; Cho, J.; Nam, W.; Karlin, K. D.; Fukuzumi, S. Electron-Transfer Reduction of Dinuclear Copper Peroxo and Bis-Mu-Oxo Complexes Leading to the Catalytic Four-Electron Reduction of Dioxygen to Water. *Chem-Eur J* **2012,** *18*, 1084-1093.
(18) Fukuzumi, S.; Tahsini, L.; Lee, Y. M.; Ohkubo, K.; Nam, W.; Karlin, K. D. Factors That Control Catalytic Two- Versus Four-Electron Reduction of Dioxygen by Copper Complexes. *J. Am. Chem. Soc.* **2012,** *134*, 7025-7035.
(19) Kakuda, S.; Rolle, C. J.; Ohkubo, K.; Siegler, M. A.; Karlin, K. D.; Fukuzumi, S. Lewis Acid-Induced Change from Four- to Two-Electron Reduction of Dioxygen Catalyzed by Copper Complexes Using Scandium Triflate. *J. Am. Chem. Soc.* **2015,** *137*, 3330-3337.
(20) Thorum, M. S.; Yadav, J.; Gewirth, A. A. Oxygen Reduction Activity of a Copper Complex of 3,5-Diamino-1,2,4-Triazole Supported on Carbon Black. *Angew. Chem. Int. Ed.* **2009,** *48*, 165-167.
(21) Wang, J.; Wang, K.; Wang, F. B.; Xia, X. H. Bioinspired Copper Catalyst Effective for Both Reduction and Evolution of Oxygen. *Nat. Commun.* **2014,** *5*.
(22) Thorseth, M. A.; Letko, C. S.; Tse, E. C. M.; Rauchfuss, T. B.; Gewirth, A. A. Ligand Effects on the Overpotential for Dioxygen Reduction by Tris(2-Pyridylmethyl)Amine Derivatives. *Inorg. Chem.* **2013,** *52*, 628-634.
(23) Goenaga, G. A.; Foister, S.; Belapure, A.; Byrne, K.; Hawks, S.; Papandrew, A. B.; Zawodzinski, T. Pyrolyzed Copper-Based Catalyst with High Oxygen Reduction Activity for Pem Fuel Cell Applications. *ECS Electrochem. Lett.* **2014,** *3*, F68-F71.
(24) Ward, A. L.; Elbaz, L.; Kerr, J. B.; Arnold, J. Nonprecious Metal Catalysts for Fuel Cell Applications: Electrochemical Dioxygen Activation by a Series of First Row Transition Metal Tris(2-Pyridylmethyl)Amine Complexes. *Inorg. Chem.* **2012,** *51*, 4694-4706.
(25) Aznar, E.; Ferrer, S.; Borras, J.; Lloret, F.; Liu-Gonzalez, M.; Rodriguez-Prieto, H.; Garcia-Granda, S. Coordinative Versatility of Guanazole [3,5-Diamino-1,2,4-Triazole]: Synthesis, Crystal Structure, Epr, and Magnetic Properties of a Dinuclear and a Linear Trinuclear Copper(Ii) Complex Containing Small Bridges and Triazole Ligands. *Eur. J. Inorg. Chem.* **2006**, 5115-5125.
(26) Kato, M.; Kimijima, K.; Shibata, M.; Notsu, H.; Ogino, K.; Inokuma, K.; Ohta, N.; Uehara, H.; Uemura, Y.; Oyaizu, N., *et al.* Deprotonation of a Dinuclear Copper Complex of 3,5-Diamino-1,2,4-Triazole for High Oxygen Reduction Activity. *Phys. Chem. Chem. Phys.* **2015,** *17*, 8638-8641.
(27) Barile, C. J.; Tse, E. C. M.; Li, Y.; Sobyra, T. B.; Zimmerman, S. C.; Hosseini, A.; Gewirth, A. A. Proton Switch for Modulating Oxygen Reduction by a Copper Electrocatalyst Embedded in a Hybrid Bilayer Membrane. *Nat. Mater.* **2014,** *13*, 619-623.
(28) McCrory, C. C. L.; Devadoss, A.; Ottenwaelder, X.; Lowe, R. D.; Stack, T. D. P.; Chidsey, C. E. D. Electrocatalytic O2 Reduction by Covalently Immobilized Mononuclear Copper(I) Complexes: Evidence for a Binuclear Cu2o2 Intermediate. *J. Am. Chem. Soc.* **2011,** *133*, 3696-3699.
(29) Mezour, M. A.; Cornut, R.; Hussien, E. M.; Morin, M.; Mauzeroll, J. Detection of Hydrogen Peroxide Produced During the Oxygen Reduction Reaction at Self-Assembled Thiol-

Porphyrin Monolayers on Gold Using Secm and Nanoelectrodes. *Langmuir* **2010,** *26*, 13000-13006.
(30) Kalimuthu, P.; John, S. A. Solvent Dependent Dimercaptothiadiazole Monolayers on Gold Electrode for the Simultaneous Determination of Uric Acid and Ascorbic Acid. *Electrochem. Commun.* **2005,** *7*, 1271-1276.
(31) Revin, S. B.; John, S. A. Electropolymerization of 3-Amino-5-Mercapto-1,2,4-Triazole on Glassy Carbon Electrode and Its Electrocatalytic Activity Towards Uric Acid. *Electrochim. Acta* **2011,** *56*, 8934-8940.
(32) Hedman, J.; Nilsson, R.; Nemnonov, S. A.; Nordling, C.; Trapezni.Va; Sorokina, M. F.; Kljushni.Oi; Klasson, M. Electronic-Structure of Some Palladium Alloys Studied by Esca and X-Ray Spectroscopy. *Phys. Scr.* **1971,** *4*, 195-201.
(33) Capece, F. M.; Dicastro, V.; Furlani, C.; Mattogno, G.; Fragale, C.; Gargano, M.; Rossi, M. Copper Chromite Catalysts - Xps Structure Elucidation and Correlation with Catalytic Activity. *J. Electron. Spectrosc. Relat. Phenom.* **1982,** *27*, 119-128.
(34) Johansson, G.; Hedman, J.; Berndtsson, A.; Klasson, M.; Nilsson, R. Calibration of Electron Spectra. *J. Electron. Spectrosc. Relat. Phenom.* **1973,** *2*, 295-317.
(35) Devaraj, N. K.; Decreau, R. A.; Ebina, W.; Collman, J. P.; Chidsey, C. E. D. Rate of Interfacial Electron Transfer through the 1,2,3-Triazole Linkage. *J. Phys. Chem. B* **2006,** *110*, 15955-15962.
(36) Yagi, I.; Inokuma, K.; Kimijima, K.; Notsu, H. Molecular Structure of Buried Perfluorosulfonated Ionomer/Pt Interface Probed by Vibrational Sum Frequency Generation Spectroscopy. *J. Phys. Chem. C* **2014,** *118*, 26182-26190.
(37) Wrzosek, B.; Bukowska, J. Molecular Structure of 3-Amino-5-Mercapto-1,2,4-Triazole Self-Assembled Monolayers on Ag and Au Surfaces. *J. Phys. Chem. C* **2007,** *111*, 17397-17403.
(38) Hasegawa, T.; Shimoaka, T.; Shioya, N.; Morita, K.; Sonoyama, M.; Takagi, T.; Kanamori, T. Stratified Dipole-Arrays Model Accounting for Bulk Properties Specific to Perfluoroalkyl Compounds. *Chempluschem* **2014,** *79*, 1421-1425.
(39) Yuan, Y. H.; Yam, C. M.; Shmakova, O. E.; Colorado, R.; Graupe, M.; Fukushima, H.; Moore, H. J.; Lee, T. R. Solution-Phase Desorption of Self-Assembled Monolayers on Gold Derived from Terminally Perfluorinated Alkanethiols. *J. Phys. Chem. C* **2011,** *115*, 19749-19760.
(40) Lu, H.; Zeysing, D.; Kind, M.; Terfort, A.; Zharnikov, M. Structure of Self-Assembled Monolayers of Partially Fluorinated Alkanethiols with a Fluorocarbon Part of Variable Length on Gold Substrate. *J. Phys. Chem. C* **2013,** *117*, 18967-18979.
(41) Wilhelm, E.; Battino, R. Thermodynamic Functions of Solubilities of Gases in Liquids at 25 Degrees C. *Chem. Rev.* **1973,** *73*, 1-9.

Table of Contents Graphic.